GOLD OXIDE FILMS GROWN IN THE CONFINED AQUEOUS LAYER BETWEEN GOLD AND ORGANIC SOLVENTS.

L.M. Gassa[a], J.O. Zerbino[a]*, A. Meyra[b], M.G. Sustersic[c], S. Siboni[d], C. Della Volpe[d].

[a]*Instituto de Fisicoquímica INIFTA.C.C. 16, Suc. 4, La Plata 1900, Argentina.*
[b]*IFLYSIB,(UNLP, CONICET, CICPBA) C.C. 565, La Plata1900, Argentina.*
[c]*FICES.25 Mayo N° 384, Villa Mercedes, San Luis 5730, Argentina.*
[d]*Dep. of Civil, Environmental and Mechanical Engineering (DICAM), Univ. of Trento, Trento 38123, Italy.*

Abstract

The properties of anodic passive films potentiostatically formed on polycrystalline gold in aqueous phosphate solutions were studied using voltammetry, electrochemical impedance spectroscopy, and contact angle measurements. The nature of the gold oxide layer was analyzed as a function of a potential holding in the aqueous double layer charge region at the interface between gold and the aqueous layer confined by insoluble organic solvents (hexane, chloroform, anisole, butyl acetate, xylene, and isopropyl ether). Different growth conditions change the homogeneity of the oxide layer leading to different passive properties. A synergetic effect on the gold oxidation of hydrogen dissolved in both the bulk metal and the confined aqueous layer is discussed.

Keywords: Gold oxide, Electrochemical impedance spectroscopy, Contact angle, Hydrogen.

* Corresponding author. Tel./fax: +542214254642.

E-mail address: jzerbino@inifta.unlp.edu.ar (J.O.Zerbino)

INTRODUCTION

Gold and gold nanoparticles are employed either as substrate or additive in electrochemical sensors in order to improve the analytical selectivity of membranes. On the other hand, drops of organic solvents immiscible in water work as template for the production of gold nanoparticles [1-5]. Besides, the contact angle (CA) of captive drops (CD) allows evaluation of the surface energy, as in the case of nanofiltration, and the development of less fouling membrane materials [6-7]. The CD technique involves placing bubbles or droplets against a solid surface where they are held captive in a cell filled with some immiscible fluid. The effect of the electrochemical potential on the surface properties of electrodes and membranes can be measured “in situ”. Under these

conditions the complete hydration of the surface avoids hydrophobic contributions to the surface tension produced by adsorbed air or empty vacuoles [8-10].

This paper investigates the effect of the applied potential program on the structure of oxide films formed on gold using voltammetry, electrochemical impedance spectroscopy (EIS) and CA measurement. The anodization is carried out in both phosphate solutions at pH 6.7 and in the same electrode in contact with the confined water layer forms when the metal is covered by several organic immiscible solvents. The comparison of the capacitance obtained in different growth conditions contributes to providing a deep insight into the different processes involved in the catalytic behavior of this complex interface.

EXPERIMENTAL

The experimental set-up has been described in previous works [11-13]. Polycrystalline gold rods (99.999% purity, area 0.5 cm^2) were used as working electrodes. Before each experiment, the electrodes were mechanically polished to a mirror finish with alumina of 0.3 and 0.05 μm. The counter electrode was a platinum wire placed around the working electrode. A Pt/H_2 electrode coupled to a Luggin-Haber capillary tip was used as reference electrode for all potential measurements.

The experiments were performed at room temperature and under bubbling nitrogen in phosphate buffer solutions of 0.25 M K_2HPO_4 + 0.25 M KH_2PO_4 pH 6.7 with and without the addition of a drop of different insoluble organic solvent like hexane, chloroform, butyl acetate, *m*-xylene, benzene, toluene and anisole. In all the cases the electrode was horizontally dipped into the solution and covered by the drop of solvent that tends to float in the electrolyte solution. Only in the case of chloroform, due to its higher density, the electrode was placed at the bottom of the cell and then became covered by the sunken drop.

The fresh polished electrode dipped in the cell was scanned by five cycles from the potentials E_c= 0.04 V up to E_a= 1.7 V at a sweep rate v = 0.1 V s^{-1} followed by a holding at open circuit E_{oc}= 0.6 V.

In the case of CA measurements a drop of solvent was introduced in the cell at E_{oc} using a micro syringe and the image of the bubble was registered by optical magnification. The CA was then calculated by the programme ImageJ and an appropriate subroutine plug-in [14-17]. Finally, several measurements were performed

holding at different potentials in the 0.04 V ≤ E ≤ 1.2 V potential range for 5 min and during the growth of the gold oxide monolayer at 1.7 V.

The impedance measurements were carried out using a Zahner Im6d. EIS were started in the frequency range of 65 kHz ≤ ω ≤ 1 MHz at the E_{OC} potential. After a holding of about τ = 20 sec at E= 0.6 V stationary values of the current were obtained. The EIS data and the current i were simultaneously recorded. Similar EIS data were obtained in the double layer potential region and during the growth of the gold oxide monolayer at 1.7 V, starting after a time of τ = 3, 10, and 20 min. Two potential programs were employed. Program 1, labeled "DL holding and 1.7 V" involved successive holds of 10 min in steps of 0.1 V towards cathodic and anodic E potentials in the double layer charge region, that is, in the 0.6 V ≥ E ≥ 0.04 V and then in 0.6 ≤ E ≤ 1.2 V potential regions. Next, the three successive EIS spectra at 1.7 V were taken. Program 2, labeled "OC and 1.7 V": after measuring at E_{OC} = 0.6 V, the three EIS spectra at 1.7 V were taken. La parte de Program 1 estaba igual y para mi no quedaba claro, la redactè nuevamente; redactarìa Program 2 nuevamente tambien como para sacarle los dos puntos Comparative measurements were made with the cycled gold electrode totally covered with a larger drop of the different organic solvents.

RESULTS

Voltammetric Data

Fig. 1 shows the simultaneous current, *i,* and the potential, *E*, detection during repetitive cycling at 0.1 V/s with the formation (anodic scan peak) and reduction (cathodic scan peak) of the Au_2O_3 monolayer.

When at the end of the anodic scan the potential is held at E_a= 1.7 V, *i* decreases rapidly in the time τ from 450 μA to less than 20 μA after 20 s (see arrow). During the subsequent cathodic scan, narrower reduction peaks result with only a very small current increase after longer holding times at 1.7 V with τ = 2, 10 and 20 min (dashed curves).

Contact angle measurements

Fig. 2 shows a plot of the contact angle θ vs. radius R plot of several immiscible solvents dipped in the buffer solution. The plotted radius concerns immiscible drops spontaneously detached from the micro syringe dipped in the phosphate solution. For all the solvents the angle is very high with values between 150 and 180 degrees. In spite of

the dispersion on the results, a tendency to reduce the angle with increasing radius is observed. The highest measured contact angle corresponds to the anisole and the lowest to the isopropyl ether drop.

Electrochemical Impedance Spectroscopy Data

Fig. 3 shows the Nyquist and the Bode ϕ vs. ω plots of the spectra obtained on gold at E_{oc}= 0.60 V and those at 1.7 V starting after a holding time of either τ=3, 10 or 20 min. The Bode impedance diagram exhibits a capacitive semicircle (3a -c) at high frequencies followed by another incompletely defined contribution at intermediate or low frequencies ($\omega \leq$ 0.1 Hz). Previously reported EIS results on gold in 0.5 M $HClO_4$ show very similar diagrams [18].

For the electrode initially held at 0.6 V and then at 1.7 V the Nyquist plots show decreasing curvature and this tendency still continues for longer times τ at 1.7 V. The decrease in the curvature is stressed when the electrode remains in the potential region 0.04 V $\leq E \leq$ 1.2 V for more than 60 min.

All the impedance experimental data can be well described by the following transfer function:

$$Z(j\omega) = R_{\Omega} + \frac{1}{[\mathrm{CPE}]_1 + (R_{t1} + Z')^{-1}} \qquad (1)$$

where $\omega = 2\pi f$. The high frequency limit R_Ω corresponds to the ohmic resistance of the electrolyte, whereas $[\mathrm{CPE}]_1$ denotes the constant phase element given by $[\mathrm{CPE}]_1 = [C_1 (j\omega)^{\alpha 1}]^{-1}$, C_1 is the capacitance at high frequencies, α_1 takes into account the distribution of the time constants due to surface inhomogeneities, and R_{t1} is the charge transfer resistance probably related to proton reduction [19]. Z' is associated with a diffusion process [13].

$$Z' = Z_w = R_{DO} (jS)^{-1/2} \tanh (jS)^{-1/2} \qquad (2)$$

where the diffusion resistance R_{DO} is the limit of $Z_w (j\omega)$ at $\omega \rightarrow 0$ and the parameter $S = d^2(\omega/D)$, being D the diffusion coefficient. This diffusion process probably occurs in the aqueous solution.

Non-linear least square fitting routines [20] provide good agreement between experimental results and simulated data. C_1 and R_{t1} values are determined from the optimum fit procedure in the region of high frequencies, obtaining C_1 = 104 ± 10 μF

cm^{-2} and $\alpha_1 = 0.94 \pm 0.02$, while R_{t1} values are in the range $14200 \leq R_{t1} \leq 78000\ \Omega\ cm^{-2}$. A clear increase in R_{t1} results during the potential holding at 1.7 V. This effect is stressed when a previous holding in the double layer region is applied (Table 1).

Similar experiments are shown for the gold electrode covered with an extended drop of either hexane (Fig. 4) or chloroform (Fig. 5). For increasing holding time at 1.7 V analogous trends in R_{t1} *are observed. However, a remarkable and unexpected split in the Bode plot is noticed at about 4 Hz (see arrow in Figs 4a, b and 5a, b). This is practically unseen in the Nyquist plot, where the capacitive semicircle is only slightly distorted. In the same way, any change is noticed in the Bode modulus plot (not shown), which remains invariable in the high frequency range and independent of the application of Procedure 1 or 2.*

Table 2 shows the fitted C_1, C_2, R_{t1} *and* R_{t2} *values obtained in the region of high frequencies using equation 1 with the transfer function Z':*

$$Z' = \frac{1}{[CPE]_2 + R_{t2}^{-1}} \qquad (3)$$

where $[CPE]_2 = [C_2 (j\omega)^{\alpha 2}]^{-1}$ *[20].*

The data show a general increase in R_{t1} and R_{t2} during the holding time at 1.7 V. The higher values in R_{t2} can be assigned to the higher passivity of the aged gold oxide patches [18].

The capacitance C_1 calculated with equation 1 and associated with the loop at higher frequencies show similar values to C_1 obtained in the fittings using equation 1 and 3. The values are in agreement with previous data reported for gold [18,21-22]. The C_2 values obtained for the two peaks fittings are one order of magnitude lower than those of C_1 in agreement with capacitance values obtained for thicker gold oxide layers [18].

Fig. 6 shows the stationary currents that result after a potential holding of about 2 min. in the double layer charge region $0.04\ V \leq E \leq 1.2\ V$ and at 1.7 V. The current at anodic potentials of E_{oc} is very low and a quasi constant value of about 0.8 μA is measured. Also, increasing values of i result in about 15 μA at cathodic potential to E_{oc}.

For hexane and chloroform Figs. 4 and 5 show the Bode plots at $E_{oc} \approx 0.6$ V with a double peak corresponding to two capacitive contributions. The fitting with the second capacity loop is tentative since the poor peak resolution is a hindrance in finding a

unique solution (Table 2). The comparison of the experimental data in Figs. 4 d and 5 d shows how the inflexion of the two contributions observed at $E_{oc} \approx 0.6$ V after the holding at 1.7 V completely vanishes. On the other hand, in Figs. 4 b and 5 b the inflection observed at $E_{oc} \approx 0.6$ V by anodization progressively unfolds a new and well defined contribution that shifts to lower frequencies.

Fig. 7 shows the stationary current i at 1.7 V as a function of the holding time τ. In addition to the systematic decrease during the potentiostatization time τ, significant lower stationary currents result when the electrodes remain for longer times in the double layer region 0.04 V $\leq E \leq$ 1.2 V prior to the anodic polarization at 1.7 V.

DISCUSSION

In the potential region corresponding to the gold oxide monolayer formation, very similar voltammetric plots are obtained in buffer solution and with the electrode totally covered with the drop of the different organic solvents (Fig. 1). This indicates that the gold electrode strongly retains a layer of confined water that can achieve a thickness of several nanometers.

Only in the case of butyl acetate, a reduction of up to 30 % in the area of both the anodic and the cathodic oxide peak can be observed during cycling. This effect strongly depends on the holding time at potentials near $E_{oc} \approx 0.6$ V. This fact indicates a significant adsorption on the metal of butyl acetate dissolved in the confined water layer. Another evidence of the adsorption of butyl acetate is the significant decrease in the CPE measured in the region 0.58 V $\leq E \leq$ 1.2 V. In the solvent-free buffer solution , values of $\alpha \approx 0.94$ are measured in the regions 0.04 V $\leq E \leq$ 0.4 V and 1.2 V $\leq E \leq$ 1.6 V with a regular decrease to a minimum value of $\alpha \approx 0.90$ at 0.6 V $\leq E \leq$ 1.0 V. Similar values of α are measured in the case of anisole and xylene. However, in the case of hexane, α decreases to a minimum value of about $\alpha \approx 0.88$ and for butyl acetate even up to 0.82 at 0.6 V $\leq E \leq$ 1.0 V, showing only one wide contribution in the Bode plot.

The adsorption of aromatic molecules on free gold/ vacuum surface is generally higher than that of aliphatic molecules because of the role played by the interaction of p-orbitals with metal orbitals, in agreement with the acid-base theory of surfaces (Good - van Oss) [23]. Therefore, we can assume that the aromatic adsorption in our case is stronger than that with aliphatic compounds. However, the presence of water hinders the adsorption of organics, such as hexane and xylene, which are scantly adsorbed [24-27].

Moreover, these investigations show that butyl acetate adsorption in the presence of water is very significant and this organic solvent is used as an efficient ore extracting agent [28-31].

As the solid has a preferential affinity for the bulk phase, a thin film of the bulk fluid is retained between the sessile drop and the solid surface [32]. The wetting of the metal surface has long been the subject of much controversy and phenomena of hysteresis may arise due to the presence of this aqueous film. In the case of the air/gold/liquid interface, different CA vs. E data can be obtained in only one experiment when starting the procedure at E_{oc}. The meniscus rise can be then measured at potentials gradually different than E_{oc} in either cathodic or anodic direction from E_{oc} [33]. A period of about 2 min was required to achieve a constant and reproducible reading at each potential. More evidence of the strongly adsorbed layer of confined water is found through the CA experiments (Fig. 2). Practically no changes in CA were detected as a function of the applied potential for the different solvents. Even after polarization at 1.7 V no significant change in the contact angle was observed for drops of the various solvents. Only in the case of anisole, and after holding times longer than 10 min at 1.7 V, a decrease higher than 10 degrees in CA is detected. However, this effect depends also on the previous holding time at the 0.04 V $\leq E \leq$ 1.2 V potential range and the hysteresis effects seem to be higher than those detected for the air/gold/liquid interface.

The Laplace equation can be applied to obtain the ideal shape of the drop in practical systems when the gravity has some perceivable effects. The value $E_{öt,}$ of the Eötvös number Eo below which a standard deviation equal or higher than one degree occurs in the contact angles can be calculated as a function of the contact angle. $E_{öt}$ decreases exponentially for increasing contact angles. This shows that the difference of the contact angles measured with the spherical fitting and at the foot drop increases both for $Eo >$ $E_{öt}$ and for increasing contact angles [34].

It should be noted that the Eötvös number is defined as $Eo = R^2 \Delta\rho\, g / 2\, \gamma$, with γ= interfacial tension, $\Delta\rho$ = density difference between the two phases, g= acceleration due to gravity, and R= radius of curvature of the drop at its apex.

For angles higher than 150 degrees the deformation becomes 3 or 4 orders of magnitude higher than for angles lower than 50 degrees, assuming fixed R, $\Delta\rho$ and γvalues [34]. The calculated $\Delta\rho / \gamma$ratio shows the lowest value for anisole and the highest for isopropyl ether (Table 3) [35]. Contrary to other solvents, for butyl acetate and

isopropyl ether/ water interfaces a noticeable decrease of the air/ solvent interfacial tension comes out. On the other hand, extra small effects can arise from the electrolyte salt which can modify the γvalue. In the case of the isopropyl ether /water a γdecrease from 17.56 to 10.26 dyne. cm^{-1} is reported after the addition of 3.25 M/l acetic acid [36].

These results show that the CA lies near 180 degrees at the foot of the drop for the various immiscible solvents. More work is being done to attain accurate measurements and to calculate the contact angle for each solvent drop and the contact area independently of buoyancy effects, in order to estimate the surface energy of the water/confined water interface [17]. The hydrogen bonded network in the thin confined aqueous layer can be distorted due to strong attractive water-surface interactions [37]. Several investigations have reported the calculated thicknesses of the liquid/ liquid interfaces. The interfacial thickness increases when the surface tension decreases, e.g. anisole/air 7.8 A^o, water/air 4.49 A^o [38]. Moreover, in the case of immiscible liquid/liquid interfaces higher thicknesses are reported, e.g. hexane/water 23.50 A^o [39]. The "dipolar width" describes the distance required for a dielectric environment to change from one phase to another and research on modeling this region is required [40]. However, these predictions have largely gone untested owing to difficulties associated with probing buried interfaces.

The analysis of the impedance parameters associated with the second time constant (equation 3) denotes a complex process and the presence of overlapped peaks make the analysis difficult [20]. However, approximate values of C_1, C_2, R_{t1} *and* R_{t2} *can be calculated from the fitting data . The highest and lowest* R_{t2} *and* C_2 *values related to those observed for* R_{t1} *and* C_1 *can be ascribed to a faceting of the surface and the growth of aged gold oxide patches [18,41]. Only higher* C_2 *values result in the case of* E_{oc} *= 0.6 V pointing to strong adsorption of organic layers. More work is in progress to improve and correlate the low frequency response involving several time constants with the layer structure.*

The pathway of oxygen activation in oxidation reactions on gold catalysts has been extensively studied; however, this topic is still under discussion [42]. Oxygen addition rate is critical to leaching of gold ores and too much oxygen results in very slow leaching kinetics [43].

The selectivity and efficiency of novel metallic gold catalysts are associated with chemisorbed molecular and atomic oxygen, oxygen atoms dissolved in the bulk, and gold oxide [42,44-47]. On the other hand, reducing pre-treatments increases the catalytic activity of the samples, while oxidative treatments deactivate the catalyst [48]. The splitting in the Bode diagrams (Figs. 4b and 5b) is only shown when the holding is made in both the 0.04 V ≤ E ≤ 0.6 V and the 0.6 V ≤ E ≤ 1.2 V potential region, indicating the effect of the hydrogen absorption on the structure and faceting of the oxide anodically grown.

In spite of the progress on the characterization of electrochemical interfaces *in situ*, a consensus on the predominant reaction mechanism for the hydrogen evolution reaction (HER) on coin metals has not been reached. The Volmer reaction, $H^+ + e^- \rightarrow H_{ad}$ is usually considered faster than the subsequent steps, the Tafel reaction $2\ H_{ad} \rightarrow H_2$ and the Heyrovsky reaction $H_{ad} + H^+ + e^- \rightarrow H_2$ [49].

HER proceeds via the Heyrovsky reaction on Pt(100) and the Tafel reaction on Pt(110). The under potential deposited hydrogen state H_{upd} is observed starting at ca. 0.35 V and increases to lower potentials up to coverage $\theta \cong 1$ at overpotentials (HER) $\eta = 0$. However, the overpotential deposited hydrogen H_{opd} has been suggested to be more reactive than the H_{upd} and only the species H_{opd} takes part in the hydrogen evolution reaction. A H_{opd} of about $\theta \cong 0.18$ is reported at $\eta = 0$ V [50].

On Au(111) the surface is free of H atom at potentials above -0.4 V and the Heyrovsky mechanism prevails [51]. Recent work has shown no hydrogen evolution in the 0.1 V ≤ E ≤ 0.5 V potential range, but the metal is loaded with atomic hydrogen [19].

Besides the hydrogen absorption, other processes like oxygen reduction and phosphate adsorption can take place in the 0.1 V ≤ E ≤ 1.2 potential range. These processes are disregarded in the present discussion as the possible source of the reported effects. The dissolved oxygen is eliminated by intense nitrogen bubbling. Phosphate adsorption is a relatively reversible process with lower hysteresis than the hydrogen absorption and at low potentials Au(111) is reported as apparently adsorbate free [52-53].

Little information is available on the details of proton hydration at interfaces [54]. Calculations are reported on the first step in the hydrogen evolution reaction, which is the transfer of a proton from the solution to the electrode surface $H^+ + e^- \rightarrow H^-$, considering that the interaction of water with the metal is weak. The rate of the electron transfer depends on the hydrogen electronic level and the calculation shows similar

values for Pt and Au for distances lower than 1.4 Å. Moreover, calculations on the atomic structure and conductance in vacuum of a gold wire show that the atomic hydrogen energetically prefer to get incorporated into the wire [55].

It is well-known that the presence of H_2 promotes oxidation reactions on gold, but the mechanism of this important phenomenon is still a matter of debate. The synergistic effect observed for the co-adsorption of hydrogen and O_2 may be caused by the formation of O–H bonds that enhance the O↔Au interactions, reducing (0.15–0.30 Å) the O–Au bond lengths. The formation of a peroxo moiety is the most accepted hypothesis to explain the mechanism [54-55].

On the other hand, after hydrogen treatment the surface oxides can be formed more easily and be reduced with a greater difficulty than on the fresh gold surface. These results are attributed to hydrogen penetration into the metal lattice [56-58]. Also, at 0.7 V the surface reconstructions of the plane (100) lifts and the hydrogen absorption is higher at more anodic potentials [19].

It is well known that the degree of solubility of hydrogen is significantly lower in water than in organic solvents, and among organic solvents it is higher in aliphatic than in aromatic compounds, while generally it is higher in liquids with greater molecular sizes. Many investigations report a solubility of hydrogen 10 times higher in hexane than in water and intermediate value in polar organic solvents [59-66]. This may strongly influence the phenomenon under study, capturing a significant quantity of hydrogen and maintaining it in a very strategic position. Moreover, the solubility of hydrogen increases dramatically over bulk values when the liquid size is reduced down to 5-15 nm [65-66]. Although a very low stationary cathodic current rises in the 0.04 V ≤ E ≤ 0.6 V double layer region ,the accumulation of hydrogen in the confined aqueous layer can achieve a high local concentration in the presence of the solvent drop. The synergetic effect of the hydrogen and the subsequent anodization in the 0.6 V ≤ E ≤ 1.2 V range produce a local incipient oxidation that increases notably the inhomogeneity of the oxide monolayer grown at 1.7 V.

CONCLUSIONS

The cycled gold electrode retains a strong adsorbed aqueous thin layer in contact with immiscible solvents. The polarization at 1.7 V shows the formation of the gold oxide monolayer even for the electrode covered with the solvent. For the metal and the oxide covered electrode similar values of double layer capacity are observed. Significant

variations depending on the holding time in the double layer potential region, 0.04 V ≤ E ≤ 0.6 V are observed in the dielectric properties and the homogeneity of the gold oxide monolayer for the electrode covered with a suitable solvent. These results show the synergetic effect of hydrogen on the gold oxidation rate.

Acknowledgements

This research project was supported by the "Comisión de Investigaciones Científicas de la Provincia de Buenos Aires, CIC", the "Consejo Nacional de Investigaciones Científicas y Técnicas, CONICET", the "Universidad Nacional de La Plata" and the "Universidad Nacional de San Luis". Work was presented in the 9th ECHEMS Meeting "Electrochemistry in Particles, Droplets and Bubbles", 23-26 June 2013, Lochow, Poland, http://echems9.pl/faq.

REFERENCES

[1] A. Krishnan, Y.H. Liu, P. Cha, R. Woodward, D. Allara, E.A. Vogler. Colloids Surf. B: BioInterf. 43 (2005) 95-98.

[2] L.L. Schramm, D.B. Fisher, S. Schürch, A. Cameron. Colloids Surf. A 94 (1995) 145-159.

[3] S. Schürch, M. Lee, P. Gehr, Pure Appl. Chem. 64 (1992) 1745-1750.

[4] M.A. Habib. Langmuir 4 (1988) 1302-1304.

[5] J. Halldorsson. Tesis: Investigation of the factors influencing the wettability of conducting polymers for fluid control in microfluidic devices. Univ.Wollongong.BSc(Hons), 2007.

[6] A. Azioune, M.M. Chehimi, B. Miksa, T. Basinska, S. Slomkowski, Langmuir 18 (2002) 1150-1156.

[7] A.R. Roudman, F.A. Digiano. J. Membr. Sci. 175 (2000) 61-73.

[8] R. Wüstneck, N. Wüstneck, D Vollhardt, R Miller, U. Piso, Mater. Sci. Eng. C 8–9, (1999) 57-64.

[9] K.S. Teh, Y. Takahashi, Z. Yao, Y-W. Lu, Sens. Actuators A 155 (2009) 113-119.

[10] L. Myong-Hoon, Mol. Cryst. Liq. Cryst. 316 (1998) 329-332.

[11] J.O. Zerbino, L.J.H. Pesetti, M.G. Sustersic, J. Mol. Liq. 131–132 (2007) 185-189.

[12] J.O. Zerbino and M.G. Sustersic, Langmuir 16 (2000) 7477–7481.

[13] J.O. Zerbino, L. Gassa, J. Solid. State Electrochem. 7 (2003) 177-182.

[14] W.S. Rasband. Online Manual for the WCIF-ImageJ collection. Appendix II: Citing ImageJ and Plugins. US National Institutes of Health, Bethesda, MD. 1997–

2005. http://rsb.info.nih.gov/ij/.

[15] C. Della Volpe, M. Brugnara, D. Maniglio, S. Siboni, T. Wangdu, About the possibility of experimentally measuring an equilibrium contact angle and its theoretical and practical consequences. In: K.L. Mittal (Ed.), 4 (2006) 79-100.

[16] M. Brugnara, C. Della Volpe, S. Siboni, D. Zeni. J. Scanning Microscopies 28 (2006) 267-273.

[17] C. Della Volpe. A program for the calculation of acid-base solid Surface free energy components (2004). http://www.ing.unitn.it/devol/, SurfTen 4.3.

[18] P.S. Germain, W.G. Pell, B.E. Conway, Electrochim. Acta 49 (2004) 1775-1788.

[19] M.G. Sustersic, N.V. Almeida, A.E. Von Mengershausen, Int. J. Hydrogen Energy 35 (2010) 6063-6068.

[20] B.A. Boukamp, EQUIVCRT Equivalent Circuit, Users Manual VER, 4.51, Univ. of Twente, The Netherlands, 1993.

[21] W.R. Fawcett, Z. Kováčová, A.J. Motheo, C.A. Foss Jr, J. Electroanal. Chem., 326 (1992) 91-103.

[22] A. Sadkowski, A.J Motheo, R.S Neves, J. Electroanal. Chem. 455 (1998) 107-119.

[23] H. Dahms, M. Green, J. Electrochem. Soc. 110 (1963) 1075-1080.

[24] K. Weiss, J. Weckesser, Ch. Wöll, J. Mol. Structure: THEOCHEM 458 (1998) 143-150.

[25] D.J Davis, G. Kyriakou, R.M. Lambert, J. Phys. Chem. B 110 (2006) 11958-11961.

[26] J.R. Sambles, J.D. Pollard, G.W. Bradberry, Optics Communications. 63 (1987) 298–300.

[27] R. Abdelhedi, M.L. Bouguerra. Electrochim. Acta. 35 (1990) 273–279.

[28] X. G. Shan, Y.F. Lin, Yejin Fenxi/Metall. Anal. 31 (2011) 64-67.

[29] K. Jakubec, Š. Zdeněk. Anal. Chim. Acta. 172 (1985) 359–364.

[30] S. Nakanishi, T. Nagai, K. Fukami, K. Sonoda, N. Oka, D. Ihara, Y. Nakato. Langmuir 24 (2008) 2564-2568.

[31] E. Lust, A. Jänes, K. Lust, V. Sammelselg, P. Miidla, Electrochim. Acta. 42 (1997) 2861–2879.

[32] J.D. Malcolm, C.D. Elliott, Can. J. Chem. Eng. 58 (1980) 151-153.

[33] I. Morcos, J. Colloid Interf. Sci. 37 (1971) 410-421.

[34] J. Chatterjee, J. Colloid Interface Sci. 259 (2003) 139-147.

[35] W. Apostoluk, J. Drzymala, J. Colloids Int. Sc. 262 (2003) 483-488.

[36] F.M. Browning, J.C. Elgin, Ind. Eng. Chem. 7 (1935) 399-400.

[37] A Striolo, in: P.B. Balbuena, J.M. Seminario (Eds), Nanomaterials: Desing and Simulation, Elsevier B.V, 2007.

[38] J.M. Douillard, J. Colloid Int. Sci. 337 (2009) 307-310

[39] A.C. Yang, D. Li, Colloid Surf.A 113 (1996) 51-59.

[40] W.H. Steel, R.A. Walker, Nature 424 (2003) 296-299.

[41] M.E. Vela, J.O. Zerbino, A.J. Arvia. Thin Solid Films 233 (1993) 82-85.

[42] J. Zhu, S.A.C. Carabineiro, D. Shan, J.L. Faria, Y. Zhu, J.L. Figueiredo, J. Catalysis 274 (2010) 207-214.

[43] M.I. Jeffrey, P.L. Breuer, C.K. Chu. Int. J. Mineral Process. 72, (2003) 323-330.

[44] J.M Gottfried, N. Elghobashi, S.L.M Schroeder, K Christmann, Surf. Sci. 523 (2003) 89-102.

[45] J. Kim, E. Samano, B.E. Koel, Surf. Sci. 600 (2006) 4622-4632.

[46] J.C.F. Rodríguez-Reyes, C.M. Friend, R.J. Madix, Surf. Sci. 606 (2012) 1129-1134.

[47] A. Abad, C. Almela, A. Corma, H. García. Tetrahedron 62 (2006) 6666-6672.

[48] N. Bogdanchikova, A. Pestryakov, I. Tuzovskaya, T.A. Zepeda, M.H. Farias, H. Tiznado, O. Martynyuk, Fuel 110 (2013) 40-47.

[49] E. Skúlason, G.S. Karlberg, J. Rossmeisl, T. Bligaard, J. Greeley, H. Jónsson, J. K. Norskov. Phys. Chem. Chem. Phys, 2007, 9, 3241-3250.

[50] P.M. Quaino, M.R. gennero de Chilavo, A.C. Chilavo. Electrochim. Acta 52 (2007) 7396-7403.

[51] Y-H Fang, G-F Wei, Z-P Liu. J. Phys. Chem. C 2013,117, 7669-7680.

[52] S.U.M. Khan, G. Liu. J. Electroanal. Chem. 270 (1989) 237-252.

[53] C. Schlaup, S. Horch, Surf. Sci. 608 (2013) 44-54.

[54] E. Santos, A. Lundin, K. Pötting, P.Quaino, W. Schmickler. Phys. Rev. B 79 (2009) 235436, 1-10.

[55] M. Kiguchi, T. Konishi, S. Miura, K. Murakoshi. Nanotechnology 18 (2007) 424011, 1-5.

[56] L. Barrio, P. Liu, J.A. Rodriguez, J.M. Campos-Martin, J.L.G. Fierro, J. Phys. Chem. C111 (2007) 19001–19008.

[57] S.M. Lang, T.M. Bernhardt, R.N. Barnett, B. Yoon, U. Landman, J. Am. Chem. Soc. 131 (2009) 8939–8951.

[58] M. Lukaszewski, T. Kedra, A. Czerwinski. Electrochem Commun. 11 (2009) 978-982.

[59] U.J. Jáuregui-Haza, E.J Pardillo-Fontdevila, A.M. Wilhelm, H. Delmas, E. Brunner, J. Chem. Eng. Data, 30 (1985) 269–273.

[60] T. Katayama, T. Nitta. J. Chem. Eng. Data 21 (1976) 194–196.

[61] P. Purwanto, R. M. Deshpande, R. V. Chaudhari, H. Delmas, J. Chem. Eng. Data (1996) 41 1414–1417.

[62] M. Pera-Titus, R. El-Chahal, V. Rakotovao, C. Daniel, S. Miachon, J.A. Dalmon, ChemPhysChem. 10 (2009) 2082–2089.

[63] J.A. Waters, G.A. Mortimer, H.E Clements. J. Chem. Engineer. Data 15(1970) 174-176.

[64] J.F. Connolly, G.A. Kandalic, J. Chem. Engineer. Data 31 (1986) 396-406.

[65] V. Rakotovao, R. Ammar, S. Miachon, M. Pera-Titus, Chem. Phys. Lett. 485 (2010) 299-303.

[66] Z. Zhou, Z. Cheng, D. Yang, X. Zhou, W. Yuan, J. Chem. Eng. Data 51 (2006) 972-976.

Captions:

Fig. 1. Current i vs. potential E voltammograms in phosphate buffer solution obtained scanning at 100 mV /s between Ec= 0.04 V and either Ea= 1.7 V. Full line show the repetitive voltammogram observed after five cycles and dotted lines show different scans after holding at Ea= 1.7 V during either τ= 2, 10 or 20 min.

Fig. 2. Contact angle θ vs. radius R for drops of different inmiscible solvents dipped in phosphate solutions and in contact with the polished and cycled gold electrode.

Fig. 3. EIS measurements in aqueous buffer solution obtaining at 0.6 V (o), and after holding different times τ at 1.7 V, the EIS starts at τ = 3, 10 and 20 min. (a, b) The electrode is held at several potentials in the potential region between 0.04 V and 1.2 V before the potential holding at 1.7. (c, d) The electrode is held at OC potential, 0.6 V before the holding at 1.7. (a, c) Nyquist plots, (b, d) Bode plots. Full lines show the simulated data in the high ω range.

Fig. 4. EIS measurements as in Fig 3. for the electrode cycled in aqueous buffer solution and covered with a hexane drop.

Fig. 5. EIS measurements as in Fig 3. for the electrode cycled in aqueous buffer solution and covered with a chloroform drop.

Fig. 6. Stationary current i vs. potential E in the buffer solution and the same electrode covered with a drop of anisole: (a) in the potential region 0.01 V ≤ E ≤ 1.2 V, (b) the i evolution plot after holding time τ at 1.7 V.

Fig. 7. Time dependence of the stationary current, i, during the 1.7 V holding for the cycled electrode and for the same electrode previously held in 0.01 V ≤ E ≤ 1.2 V potential region. (a) Buffer solution and the same electrode covered with b) a hexane drop or (c) a chloroform drop.

Table 1. Parameters obtaining by fitting the equivalent circuit of equation 1 at high frequencies.

Table 2. Parameters obtaining by fitting the equivalent circuit of equation 1 and 3 at high frequencies.

Table 3. Surface tension of the different solvents, γ, and the difference of density $\Delta\rho$, between the two phases solvent/water.

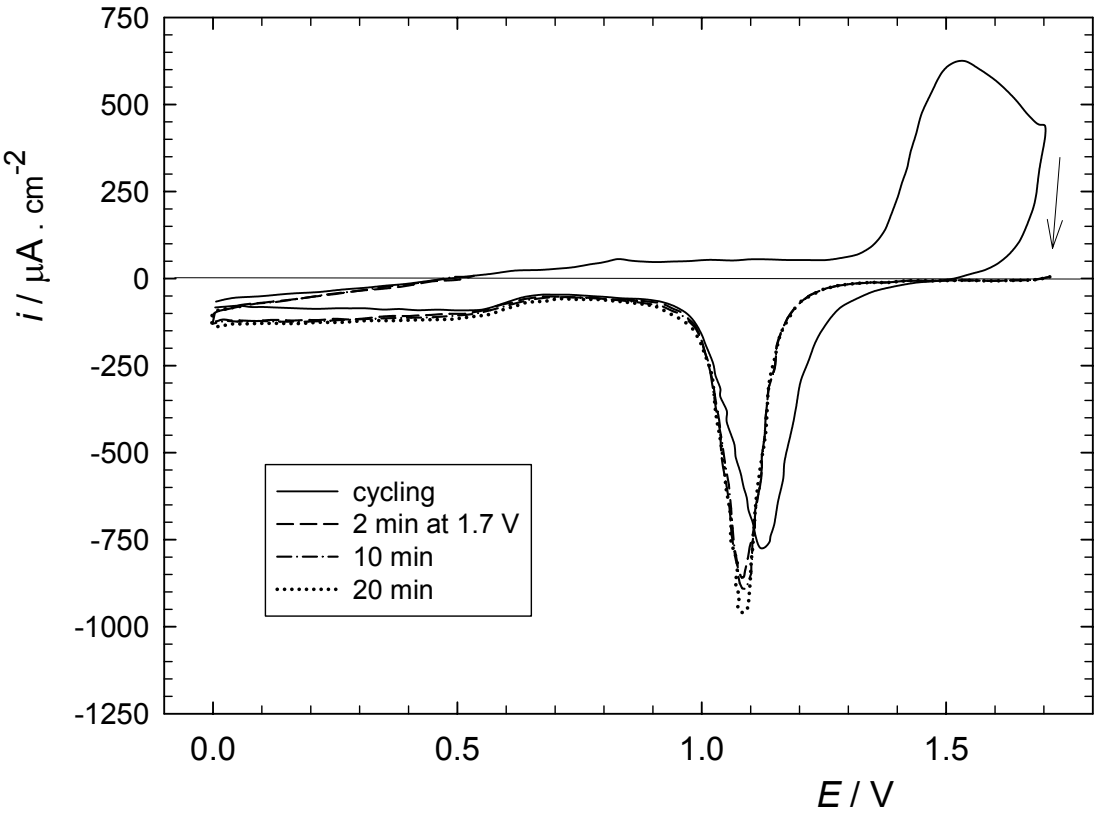

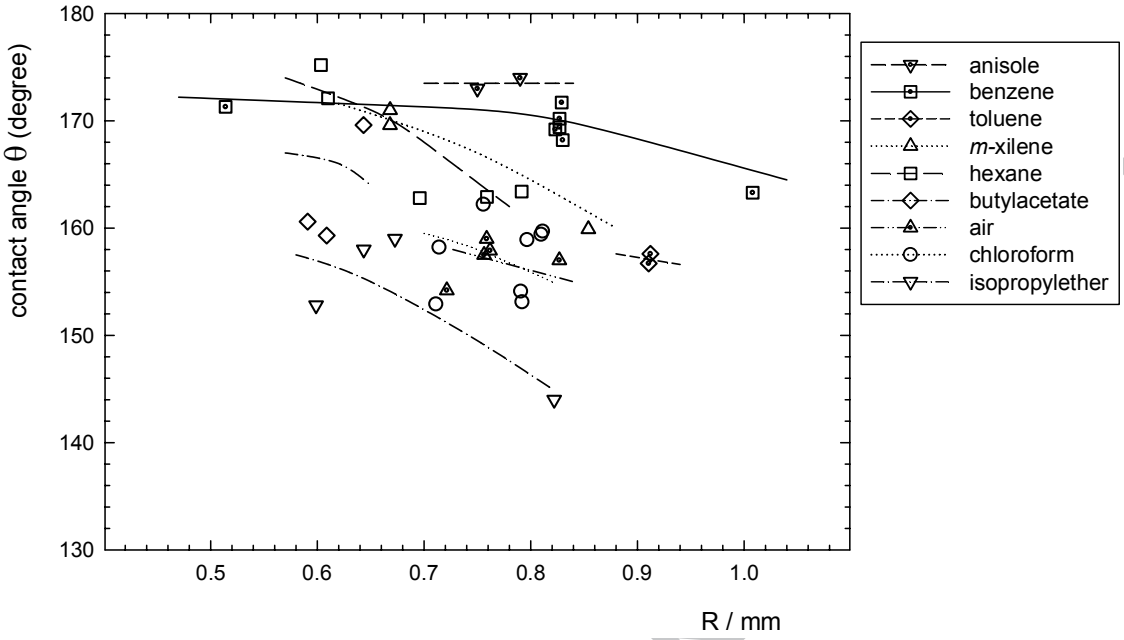

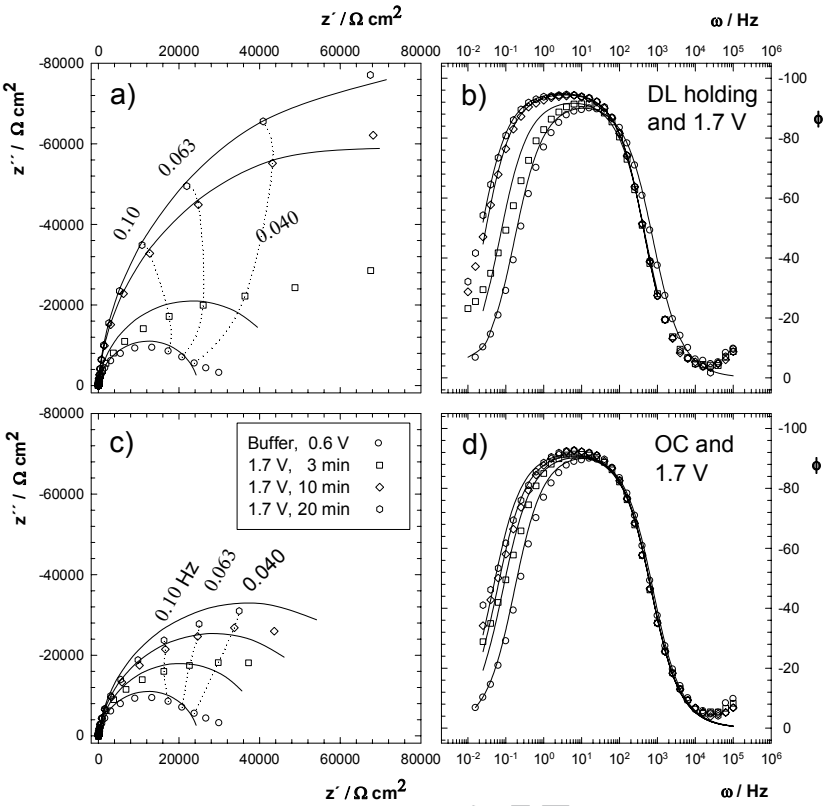

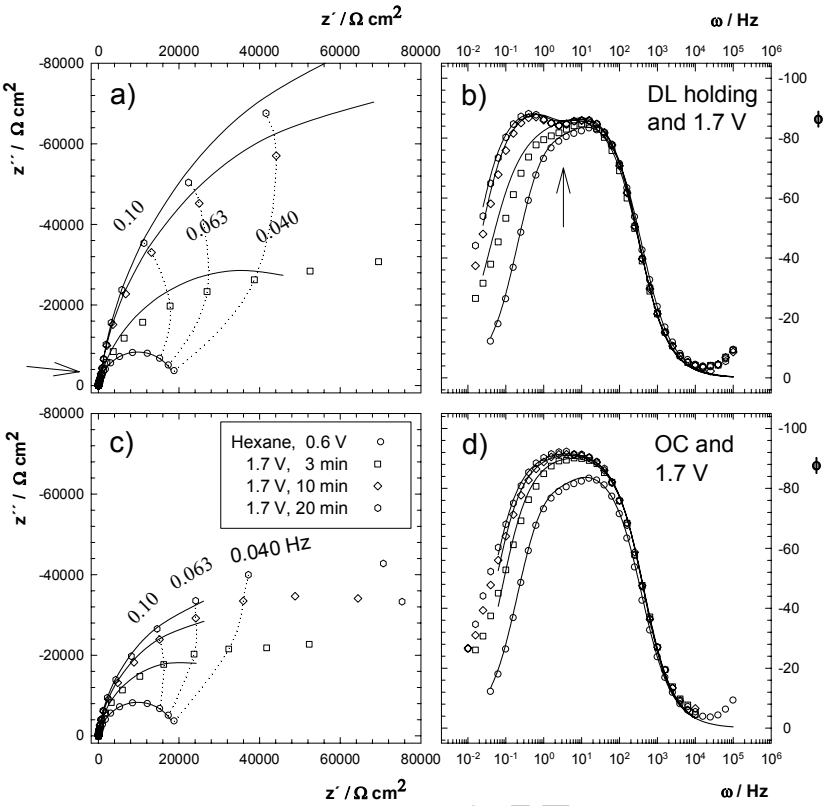

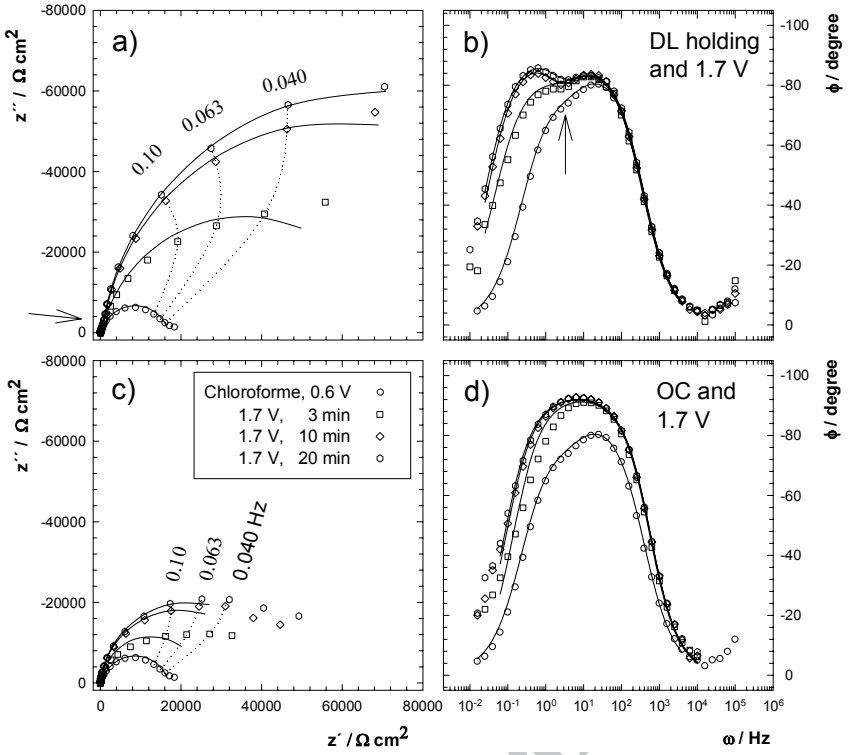

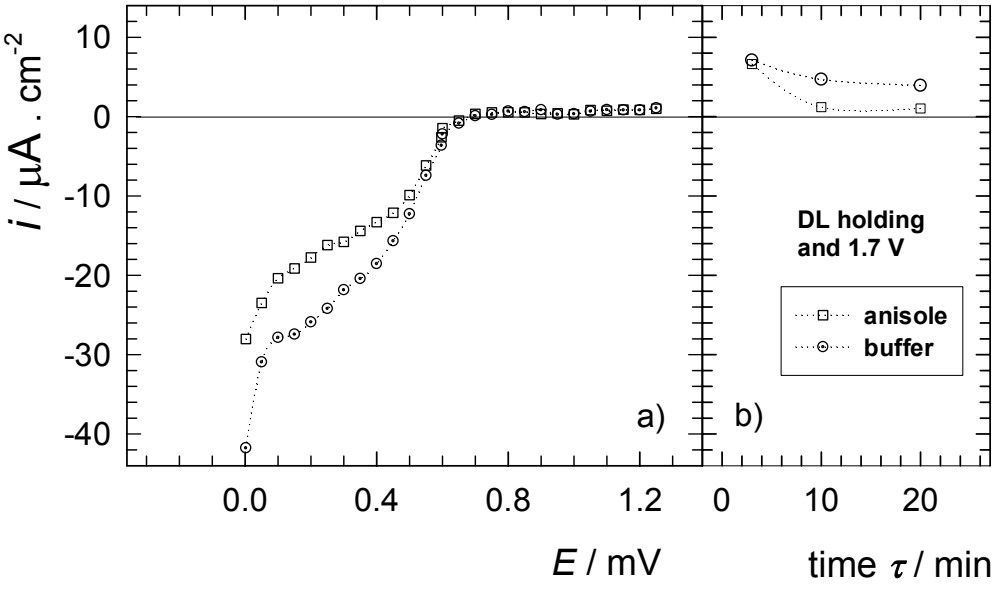

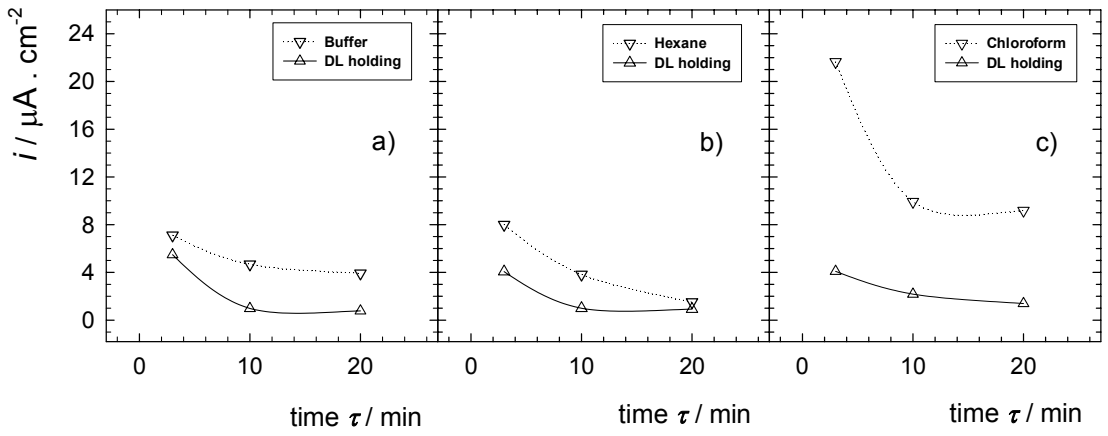

Experiment	E(V)	R(Ω.cm^2)	C_1(μF cm^{-2})	α_1	R_{t1}(Ω.cm^2)
Buffer OC and 1.7 V	0.6 V	5.19	103.56	0.92	14219
	3 min	5.04	109.58	0.93	16785
	10 min	5.05	102.30	0.94	23135
	20 min	5.07	100.56	0.94	26265
Buffer DL holding and 1.7 V	3 min	5.85	113.94	0.94	18375
	10 min	5.85	96.46	0.96	46840
	20 min	5.83	95.86	0.96	77960
Hexane OC and 1.7 V	3 min	7.06	128.64	0.92	20668
	10 min	7.15	120.98	0.93	32459
	20 min	7.25	116.68	0.93	39922
Chloroform OC and 1.7 V	3 min	5.29	115.46	0.94	12647
	10 min	5.31	108.66	0.94	19877
	20 min	5.32	107.60	0.94	22024

Table 1. Parameters obtaining by fitting the equivalent circuit R(QR) at high frequencies.

Experiment	E(V)	R(Ω.cm^2)	C_1(μF cm^{-2})	α_1	R_{t1}(Ω.cm^2)	C_2(μF cm^{-2})	α_2	R_{t2}(Ω.cm^2)
Hexane DL holding and 1.7 V	0.6 V	12.50	109.54	0.90	4661	23.40	1.00	5000
	3 min	12.85	121.54	0.90	7525	34.12	0.87	19655
	10 min	13.10	95.66	0.92	4998	13.40	1.00	69700
	20 min	13.25	84.76	0.93	4835	16.40	1.00	89900
Chloroform DL holding and 1.7 V	0.6 V	16.05	87.60	0.89	2598	157.92	0.80	5850
	3 min	15.10	80.30	0.91	1983	48.24	0.83	31030
	10 min	15.20	90.16	0.90	4731	18.16	0.99	54850
	20 min	14.15	94.38	0.90	4636	14.28	1.00	63950

Table 2. Parameters obtaining by fitting the equivalent circuit R(Q(R(QR))) at high frequencies.

Solvent	γ solvent / air dyn.cm^{-1}	γ solvent / water dyn.cm^{-1}	ρ density solvent	Δ ρ / γ
Anisole	29.31	25.8	0.995	0.0002
Benzene	28.88	35.0	0.879	0.0035
Toluene	28.40	36.1	0.867	0.0037
m-Xilene	28.90	37.9	0.860	0.0037
Hexane	18.43	51.1	0.659	0.0067
Butylacetate	25.09	14.5	0.886	0.0079
Air	73.70	72.8	0.000	0.0137
Chloroform	26.67	32.8	1.480	0.0146
Isopropylether	32.00	17.9	0.725	0.0154

Table 3. Surface tension of the different solvents, γ, and the the difference of density between the two phases solvent/water, Δρ.

Highlights

1) Gold oxide is grown in a confined aqueous layer on gold polycrystalline electrodes.
2) The contact angle of the captive drop of the organic solvents is near to 180 degrees.
3) The effect of the buoyancy effect on the contact angle is discussed.
4) After catodization the Bode diagram shows a splitting of the phase peak.
5) Hydrogen dissolved in the bulk metal and in the confined aqueous layer produces a faceting of the aged oxide.